Journal of Magnetism and Magnetic Materials 324 (2012) 1606–1612

Contents lists available at SciVerse ScienceDirect

Journal of Magnetism and Magnetic Materials

journal homepage: www.elsevier.com/locate/jmmm

Room-temperature antiferromagnetism in CuMnAs

F. Máca [a], J. Mašek [a], O. Stelmakhovych [b], X. Martí [b,c], H. Reichlová [c,b], K. Uhlířová [b], P. Beran [d], P. Wadley [c], V. Novák [c], T. Jungwirth [c,e,*]

[a] Institute of Physics ASCR, v.v.i., Na Slovance 2, 182 21 Praha 8, Czech Republic
[b] Faculty of Mathematics and Physics, Charles University in Prague, Ke Karlovu 3, 121 16 Prague 2, Czech Republic
[c] Institute of Physics ASCR, v.v.i., Cukrovarnická 10, 162 53 Praha 6, Czech Republic
[d] Nuclear Physics Institute ASCR, v.v.i., 250 68 Řež, Czech Republic
[e] School of Physics and Astronomy, University of Nottingham, Nottingham NG7 2RD, United Kingdom

ARTICLE INFO

Article history:
Received 29 September 2011
Received in revised form
23 November 2011
Available online 19 December 2011

Keywords:
Antiferromagnet
Semiconductor
Semimetal

ABSTRACT

We report on an experimental and theoretical study of CuMn–V compounds. In agreement with previous works we find low-temperature antiferromagnetism with Néel temperature of 50 K in the cubic half-Heusler CuMnSb. We demonstrate that the orthorhombic CuMnAs is a room-temperature antiferromagnet. Our results are based on X-ray diffraction, magnetization, transport, and differential thermal analysis measurements, and on density-functional theory calculations of the magnetic structure of CuMn–V compounds. In the discussion part of the paper we make a prediction, based on our density-functional theory calculations, that the electronic structure of CuMn–V compounds makes a transition from a semimetal to a semiconductor upon introducing the lighter group-V elements.

1. Introduction

Recent observation of a large magnetoresistance in an antiferromagnet (AFM) based spin-valve opens the prospect for utilizing AFMs in spintronics [1]. This motivates a search for new materials which may be suitable for spintronics and are room-temperature AFMs. In this paper we focus on CuMn–V compounds, in particular on the CuMnAs.

In the literature, CuMnSb is often quoted as a rare example among half-Heusler alloys with AFM order [2–8]. It has a relatively low Néel temperature of 50 K. Synthesis and crystal structure measurements of the lighter group-V compounds CuMnAs and CuMnP were reported in Ref. [9]. Unlike the cubic half-Heusler CuMnSb, the equilibrium crystal structure of CuMnAs and CuMnP is orthorhombic Pnma. Susceptibility measurements of CuMnAs up to room temperature presented in Ref. [9] indicated possible AFM order in this compound but the transition into the ordered state was not identified in this work. To the best of our knowledge, the CuMn–V compounds with lighter group-V elements than Sb have not been further investigated experimentally and no magnetic and electronic band structure calculations for these compounds have been published to date.

In this paper we present X-ray diffraction, magnetization, transport, and differential thermal analysis measurements of chemically synthesized CuMnAs. As a reference, we also report our measurements on CuMnSb. Experimental data are complemented by full-potential density-functional theory calculations of the magnetic structure of CuMn–V compounds. In both experiment and theory we find a large enhancement of the Néel temperature in CuMnAs as compared to CuMnSb and we associate this effect to the different crystal structures of the two compounds.

We conclude our paper by a discussion section in which the density-functional theory, which has successfully described magnetic properties of the studied CuMn–V compounds, is used to analyze the electronic band-structure character of these materials. In agreement with previous studies we obtain a semimetal-like band structure of CuMnSb [5]. For the lighter group-V elements, our calculations predict a transition into a semiconductor. We discuss this theoretical prediction in the context of the broad family of magnetic counterparts of common semiconductor compounds.

2. Experiment

In this section we discuss experimental properties of CuMnAs and provide evidence for room-temperature antiferromagnetism in the compound from magnetization, electrical transport, and differential thermal analysis measurements. Samples were prepared by

* Corresponding author at: Institute of Physics ASCR, v.v.i., Cukrovarnická 10, 162 53 Praha 6, Czech Republic.
E-mail address: jungw@fzu.cu (T. Jungwirth).

0304-8853/$ - see front matter © 2011 Elsevier B.V. All rights reserved.
doi:10.1016/j.jmmm.2011.12.017

direct synthesis from elements [10] mixed in the stoichiometric 1:1:1 ratio using Cu (purity 99.999%), Mn (purity 99.98%), and As (purity 99.999%). They were placed into Al_2O_3 crucible and double sealed inside quartz ampoules. Samples were heated up to 1000 °C at a rate of 1 °C/min and annealed for 1 day. The reaction produced silver-gray solid rocks. Elemental analysis by energy-dispersive X-ray spectroscopy (EDX) confirmed the stoichiometric 1:1:1 ratio of Cu, Mn, and As(Sb) in the studied materials within the experimental error. Powder samples and polished-layer samples were prepared from the material for X-ray diffraction measurements, chemical analysis, magnetization measurements by the superconducting quantum interference device (SQUID), and four-point transport measurements in polished 3 mm long bars with a 200 × 200 μm^2 cross-section. The differential thermal analysis (DTA) was measured on the Setaram SETSYS-2400 CS instrument. About 50 mg of the sample were enclosed in the alumina container and kept in He atmosphere while applying a constant heating/cooling rate of 5 K/min. For comparison we also prepared and measured CuMnSb samples using the same procedures.

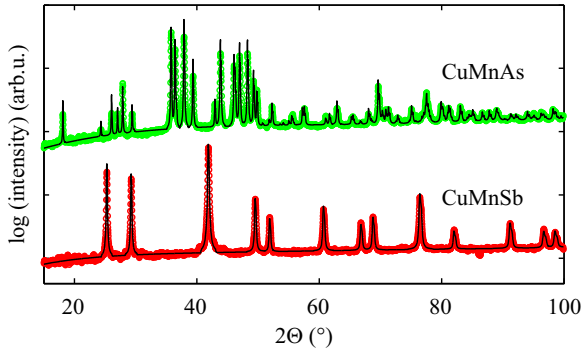

Fig. 1. X-ray diffraction data for CuMnAs and CuMnSb at room temperature. Green points are measured data of CuMnAs, red points are measured data of CuMnSb, and black thin lines are fits considering the orthorhombic Pnma crystal structure of CuMnAs and cubic crystal half-Heusler structure of CuMnSb. (For interpretation of the references to color in this figure legend, the reader is referred to the web version of this article.)

In Fig. 1 we show room-temperature X-ray measurements of our CuMnAs and CuMnSb materials. Data analysis was carried out using the FullProf package [11]. The measurements show that CuMnAs has the orthorhombic Pnma crystal structure consistent with X-ray data in Ref. [9] and CuMnSb has the cubic half-Heusler structure as reported previously [3]. Note that our X-ray measurements of CuMnAs performed in the 300–600 K range did not reveal any structural phase transition.

In the top panels of Fig. 2 we show measurements of the temperature dependent magnetic susceptibility and electrical resistivity of CuMnSb and CuMnAs. Data were collected after field-cooling the sample under 5 kOe. In agreement with previous reports on CuMnSb [3,6], both the susceptibility and resistivity data indicate $T_N \approx 50$ K for CuMnSb. The increasing magnetic susceptibility with increasing temperature, which is the signature of AFM ordering, is also observed in CuMnAs in agreement with Ref. [9]. Our measurement is, however, extended to high temperatures and we observe that the trend persists to temperatures close to ~ 400 K. This shows that the AFM transition temperature in this material is above room temperature. Consistent result is obtained from the cusp in the measured temperature dependent resistivity of CuMnAs. Note that in agreement with the AFM ordering, we find in both materials zero remanence below the transition temperature. Yet another evidence of the phase transition with the critical temperature corresponding to the one inferred from the magnetic and transport measurements in CuMnAs is obtained from the differential thermal analysis experiment (see Fig. 2). The differential thermal analysis of CuMnSb in the high temperature range did not reveal any feature, consistent with the low T_N of this material. The heat capacity measurements

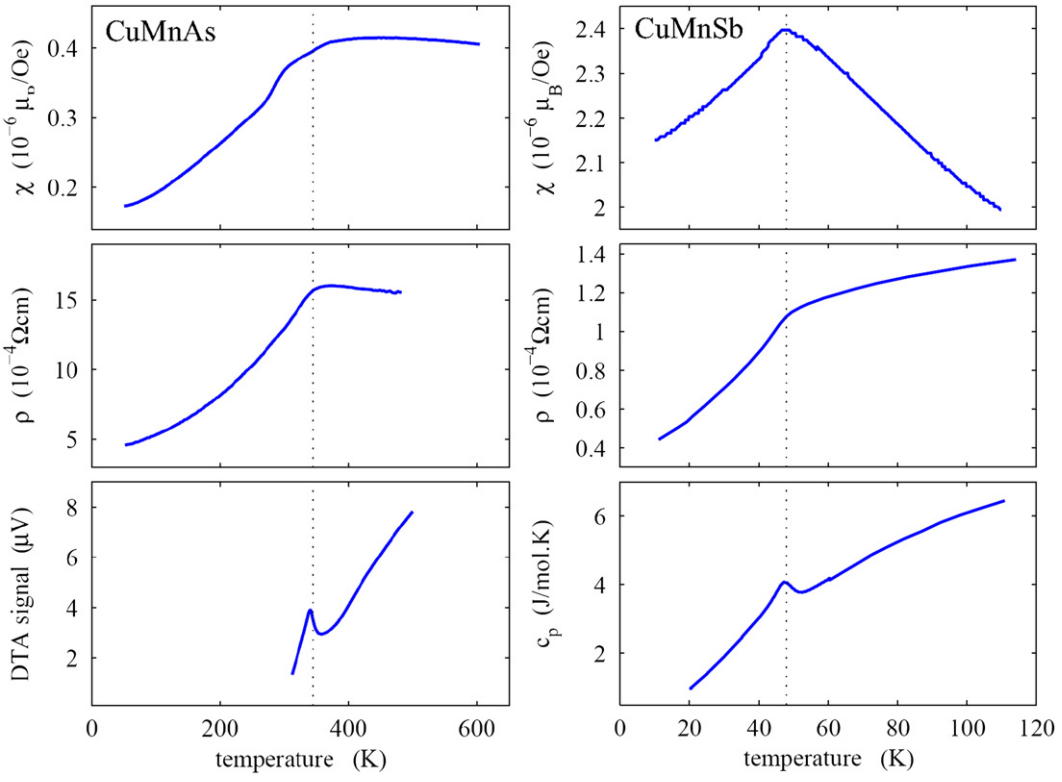

Fig. 2. Left panels: magnetic susceptibility at 5 kOe, resistivity, and differential thermal analysis measurements of CuMnAs. Right panels: magnetic susceptibility at 5 kOe, resistivity, and specific heat measurements of CuMnSb.

performed in the low temperature range confirm $T_N \approx 50$ K in CuMnSb, as shown in Fig. 2.

3. Theory

To calculate the magnetic structure of CuMn–V compounds we employed the full-potential linearized-augmented-plane-wave method (WIEN2k package) [12]. Using the generalized-gradient approximation (GGA) [13] we first compare energies of the FM and AFM states of the equilibrium orthorhombic crystal structure and the metastable cubic half-Heusler structure of CuMnAs and CuMnP. In the former case we use experimental lattice parameters [9] $a=6.5859$ Å, $b=3.8671$ Å, and $c=7.3202$ Å for CuMnAs and $a=6.3188$ Å, $b=3.7239$ Å, and $c=7.0883$ Å for CuMnP. By minimizing the total energy of the cubic phase we determined the corresponding theoretical lattice constant $a=5.83$ Å for CuMnAs and $a=5.66$ Å for CuMnP. The calculated difference between the FM and AFM total energy in the cubic crystal phase is $E_{FM}-E_{AFM}=$ 52 meV/Mn-atom for CuMnAs and $E_{FM}-E_{AFM}=59$ meV/Mn-atom for CuMnP. Here we considered the same AFM alignment of Mn moments in CuMnAs and CuMnP as reported in the neutron diffraction study of CuMnSb [2]. A comparison with theoretical results for CuMnSb, where $E_{FM}-E_{AFM}=50$ meV/Mn-atom [5], suggests that T_N increases when replacing Sb with As or P due to a tighter lattice arrangement. However, the expected increase of T_N is only in the range of $\sim 20\%$ for the cubic phase.

For the stable orthorhombic structure of CuMnAs and CuMnP we considered the FM and three different AFM moment configurations, as shown in Fig. 3. Mn atoms in these orthorhombic crystals are arranged in layers parallel to the $a-c$ plane and the different AFM arrangements can then be characterized by AFM in-plane arrangement and FM coupling between the planes ($AFM_{IP}-FM_{OP}$, Pn′m′a, Fig. 3(b)), FM in-plane arrangement and AFM coupling between the planes ($FM_{IP}-AFM_{OP}$, Pn′m′a′, Fig. 3(c)), or AFM in-plane arrangement and AFM coupling between the planes ($AFM_{IP}-AFM_{OP}$, Pnm′a, Fig. 3(d)). In CuMnAs, the GGA total energies of the $FM_{IP}-AFM_{OP}$ and $AFM_{IP}-AFM_{OP}$ states are very similar (the difference is 1 meV/Mn-atom) while the energy of the $AFM_{IP}-FM_{OP}$ state is significantly higher (by 80 meV/Mn-atom). In CuMnP, the $AFM_{IP}-FM_{OP}$ state has again the highest energy and the difference between the GGA energy of the states $FM_{IP}-AFM_{OP}$ and $AFM_{IP}-AFM_{OP}$ is 30 meV/Mn-atom with the latter AFM state having the lowest energy. When comparing total energies of the FM and AFM states we took the $AFM_{IP}-AFM_{OP}$ state, i.e. compared energies of the spin configurations in Fig. 3(a) and (d), and obtained $E_{FM}-E_{AFM}=241$ meV/Mn-atom for CuMnAs and $E_{FM}-E_{AFM}=250$ meV/Mn-atom for CuMnP. These values are significantly larger than in the cubic crystals. The theory therefore shows, in agreement with our experiment in CuMnAs, that the lighter group-V orthorhombic CuMn–V compounds have significantly higher Néel temperature than the cubic half-Heusler CuMnSb.

From our calculations it is evident that it is the orthorhombic crystal structure with layered arrangement of Mn atoms in CuMnAs which is responsible for the large enhancement of the Néel temperature in this compound, as compared to the half-Heusler CuMnSb. We interpret this as a consequence of the removed magnetic frustration associated with the crystal transition from the cubic half-Heusler to the layered orthorhombic phase. In Fig. 4 we show the AFM coupling of the (111) planes of the half-Heusler CuMnSb in which we highlight the frustration in the magnetic order within the Mn nearest-neighbor triangles. This frustration is not present in the orthorhombic CuMnAs.

The stability of the orthorhombic crystal phase of CuMnAs and CuMnP and the possibility for these compounds to form thin epitaxial films with the metastable cubic half-Heusler phase can be estimated from the difference in total energies of the two crystal structures. For CuMnAs we obtained $E_{cubic}-E_{ortho}=0.56$ eV/Mn-atom and for CuMnP the difference is $E_{cubic}-E_{ortho}=1.18$ eV/Mn-atom. For comparison, the total energy of the cubic phase of, e.g., GaN is larger than the energy of the equilibrium hexagonal phase by 0.02 eV/atom and in this case both crystal structures can be realized in thin films. For MnAs on the other hand, the difference between the cubic and hexagonal phases is 1 eV/Mn-atom and the cubic phase has been stabilized only in the form of nanocrystal inclusions in a cubic matrix. From these comparisons we conclude that the orthorhombic phases of CuMnAs and CuMnP are very stable and the occurrence of the metastable cubic half-Heusler phases in bulk or thin film materials is unlikely.

4. Discussion

Room-temperature AFMs are particularly appealing in the context of semiconductor spintronics because of the lack of suitable

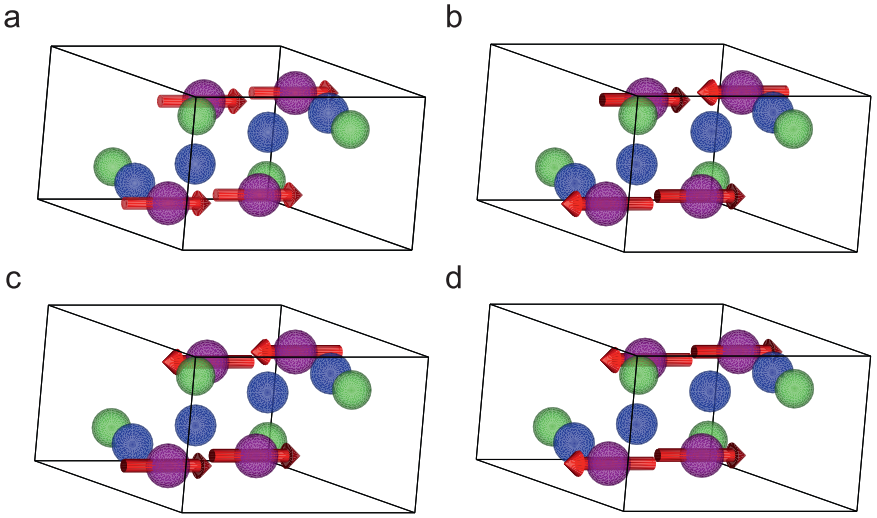

Fig. 3. Atomic and magnetic arrangements of the orthorhombic CuMnAs(P). Purple (large) spheres with arrows represent Mn, blue (medium) spheres Cu, and green (small) spheres As. (a) FM in-plane arrangement and FM coupling between the planes, (b) AFM in-plane arrangement and FM coupling between the planes, (c) FM in-plane arrangement and AFM coupling between the planes, (d) AFM in-plane arrangement and AFM coupling between the planes. (For interpretation of the references to color in this figure legend, the reader is referred to the web version of this article.)

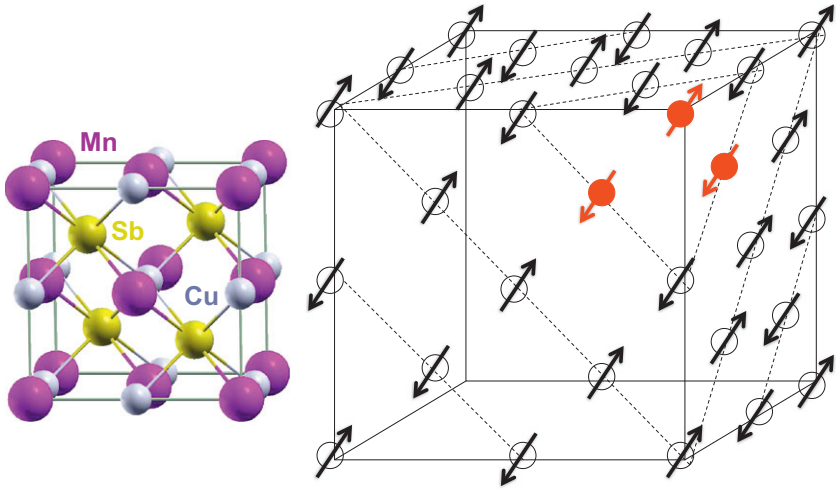

Fig. 4. Schematics of the cubic half-Heusler crystal structure of CuMnAs and of the AFM magnetic arrangement of the Mn moments. The frustrated magnetic coupling is highlighted in red. (For interpretation of the references to color in this figure legend, the reader is referred to the web version of this article.)

Table 1
Comparison of FM Curie temperatures (T_c) and AFM Néel temperatures (T_N) of II–VI, I–VI–III–VI, III–V, and II–V–IV–V magnetic semiconductors.

II–VI	T_c (K)	T_N (K)		III–V	T_c (K)	T_N (K)	
MnO		122	[15]	FeN		100	[16]
MnS		152	[17]	FeP		115	[18]
MnSe		173	[15]	FeAs		77	[19]
MnTe		**323**	[15]	FeSb		100–220	[20]
EuO	67		[15]	GdN	72		[15]
EuS	16		[15]	GdP		15	[21]
EuSe		5	[15]	GdAs		19	[22]
EuTe		10	[15]	GdSb		27	[23]
I–VI–III–VI				II–V–IV–V			
$CuFeO_2$		11	[24]	$MnSiN_2$		**490**	[25]
$CuFeS_2$		**825**	[15]				
$CuFeSe_2$		70	[26]				
$CuFeTe_2$		254	[27]				

high-temperature ferromagnetic (FM) semiconductors [14]. In this section we present our density-functional calculations of the electronic structure of the CuMn–V compounds which suggest a transition from a semimetal to a semiconductor band structure in the lighter group-V CuMn–V materials. We discuss the results in the context of the broad family of magnetic semiconductor compounds.

In Table 1 we show a survey of the magnetic counterparts of the most common II–VI and III–V compound semiconductors, and of the related I–VI–III–VI and II–V–IV–V families, in which Mn (Eu) acts as a group-II atom and Fe (Gd) as a group-III element. The table illustrates that AFM ordering occurs much more frequently than FM ordering. Yet, only a few of these AFM semiconductors have Néel temperatures above room temperature. In MnTe, T_N=323 K is presumably still too low to allow for room-temperature applications of the material in spintronics. $MnSiN_2$ appears as an attractive candidate material which should also allow for the application of common molecular beam epitaxy techniques for the synthesis of high quality films. The natural mineral $CuFeS_2$ is more challenging from the perspective of the epitaxial growth because of the vastly different vapor pressures of S and transition metals. Another limiting factor is that both $MnSiN_2$ and $CuFeS_2$ might be the only high-T_N AFMs in their respective semiconductor compound families.

The search for other high temperature AFM semiconductors has recently resulted in a report of the semiconducting band

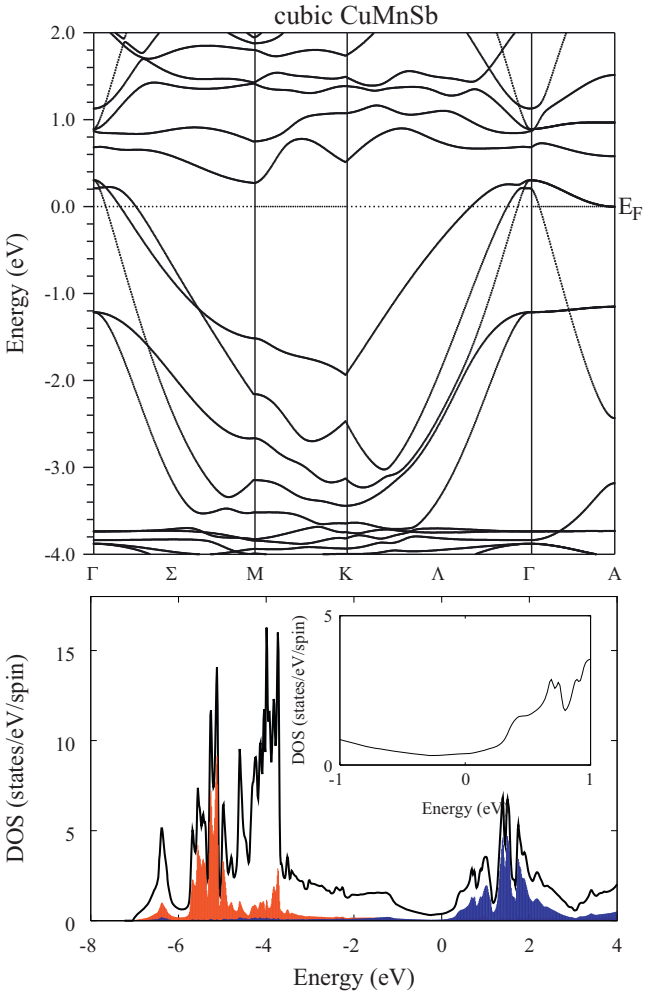

Fig. 5. GGA+U band structure plotted along lines in a hexagonal Brillouin zone (upper panel) and density of states (DOS) of cubic CuMnSb. The red (filled lower energy) data correspond to the DOS projected onto spin-up (spin-down) states of the 1st (2nd) Mn sublattice; the blue (filled higher energy) data correspond to the DOS projected onto spin-down (spin-up) states of the 1st (2nd) Mn sublattice. (For interpretation of the references to color in this figure legend, the reader is referred to the web version of this article.)

structure of alkali-metal I(a)–Mn–V compounds and of the successful synthesis of single-crystal LiMnAs by molecular beam epitaxy [14]. In contrast to the other common semiconductor compound families, many of the I(a)–Mn–V semiconductors are room-temperature AFMs [10,28]. While favorable from the perspective of their electronic band structure and magnetic characteristics, the utility of I(a)–Mn–V materials in devices may represent a challenge due to the high reactivity and diffusivity of the I(a) alkali metals elements.

The anticipation of semiconducting band structure of the high-temperature AFM LiMnAs (and other I(a)–Mn–V's) was based on the picture of Li^{1+} charge state as in Zintl compounds, Mn^{2+} charge state as observed in (Ga,Mn)As and some other (III,Mn)V and (II,Mn)VI magnetic semiconductors, and the established close relationship between non-magnetic I(a)–II–V and III–V semiconductors [14]. From this perspective, the $Cu^{1+}Mn^{2+}Sb^{3-}$ configuration inferred from previous density-functional theory studies [5] hints that the replacement of the I(a) alkali-metal with the I(b) Cu in I–Mn–V compounds may also yield a semiconducting band structure, at least for the lighter group-V compounds.

Although not a semiconductor, CuMnSb is not a conventional metal with a high density of states at the Fermi energy but rather a semimetal with a small overlap between the bottom of the conduction band and the top of the valence band [5,8]. The relatively low conductivity of this compound supports the theoretically predicted semimetal band-structure [6]. By introducing a lighter group-V element As or P, one may expect the band-gap to fully open.

Examples of our calculated band dispersions of the CuMn–V compounds are shown in Figs. 5–9. In Figs. 5 and 6 we compare band structures of the cubic CuMnSb and CuMnP calculated in the GGA+U approximations with typical values of the correlation parameters [29,30] for Mn d-orbitals, $U=3.5$ eV and $J=0.6$ eV. As already pointed out in Ref. [5], CuMnSb is a semimetal with a negative indirect band-gap. Fig. 6 shows that CuMnP, on the other hand, is already a semiconductor with a fully developed positive band-gap throughout the entire Brillouin zone. The semiconducting band structure of CuMnP is obtained also in the GGA+U calculation of the orthorhombic phase as shown in Fig. 7.

The orthorhombic CuMnAs has a small but non-zero density of states at the Fermi energy in the GGA+U spectra as shown in Fig. 8. Since density-functional theory tends to underestimate band gaps in semiconductors we conclude that the electronic structure of CuMnAs is in the transition region between a semimetal and a semiconductor. For completeness we compare in Fig. 9 band structures of orthorhombic CuMnAs and CuMnP calculated in the local density approximation (LDA) [31], LDA+U, GGA, and GGA+U. In the plots we focus on the part of the spectra

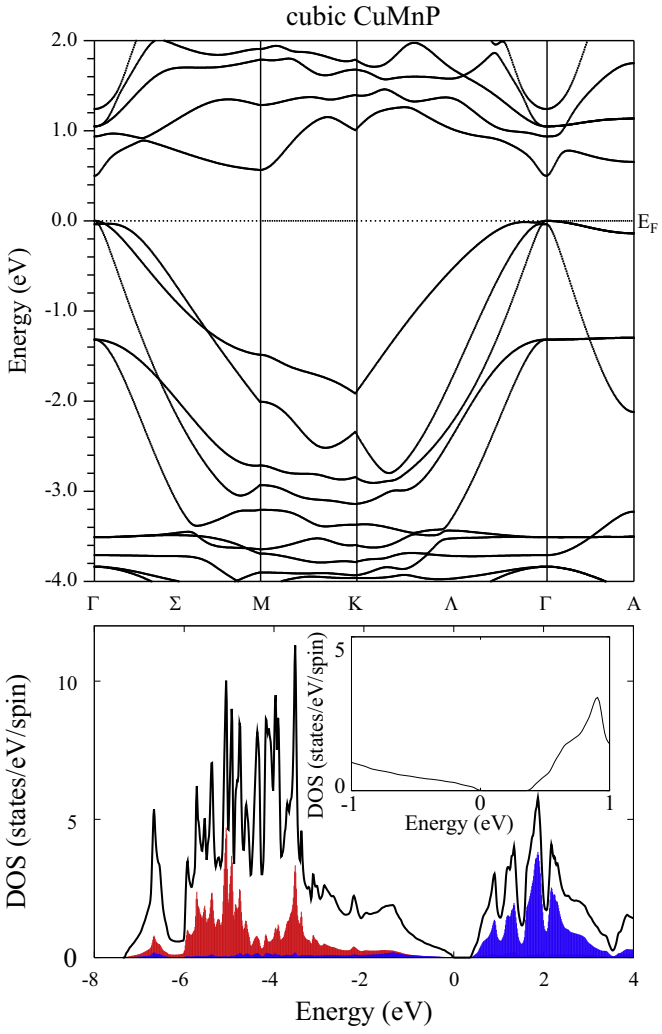

Fig. 6. Same as Fig. 5 for cubic CuMnP.

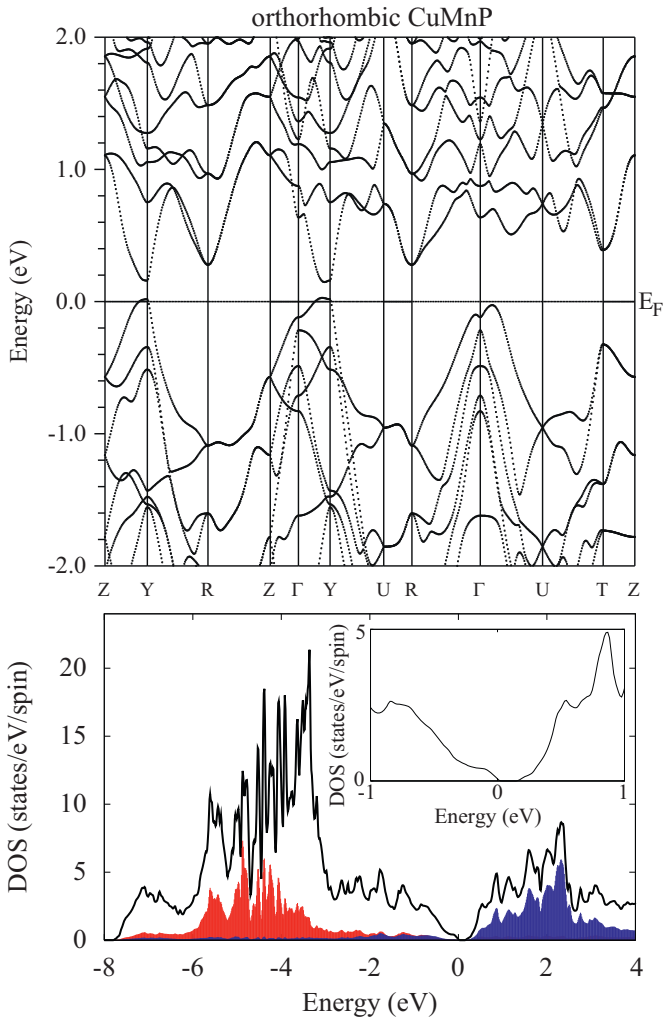

Fig. 7. GGA+U band structure (upper panel) and density of states (DOS) of orthorhombic CuMnP. The red (filled lower energy) data correspond to the DOS projected onto spin-up (spin-down) states of the 1st (2nd) Mn sublattice; the blue (filled higher energy) data correspond to the DOS projected onto spin-down (spin-up) states of the 1st (2nd) Mn sublattice. (For interpretation of the references to color in this figure legend, the reader is referred to the web version of this article.)

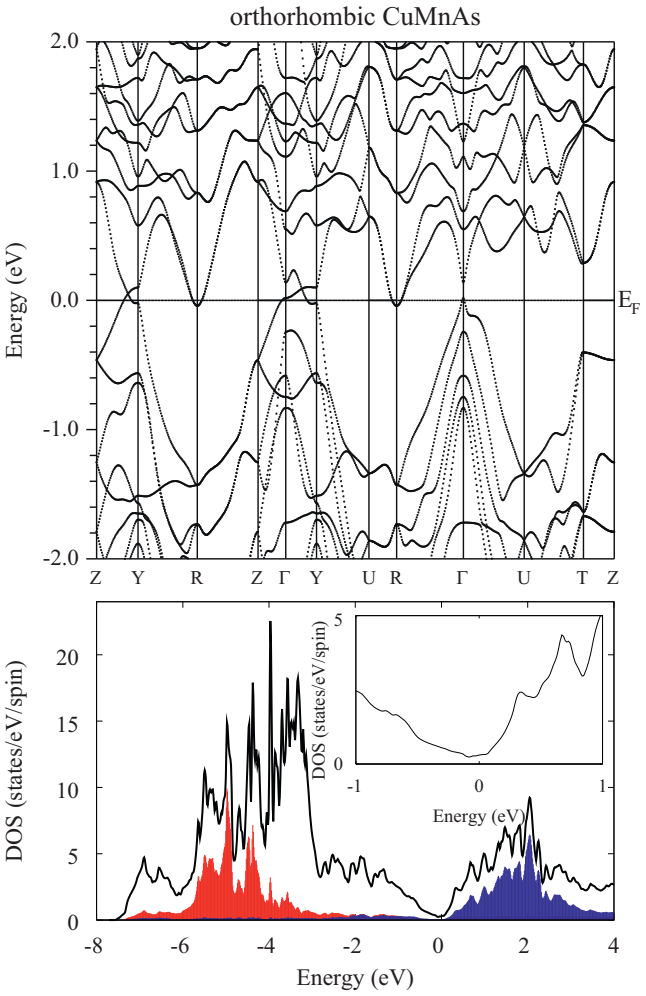

Fig. 8. Same as Fig. 7 for orthorhombic CuMnAs.

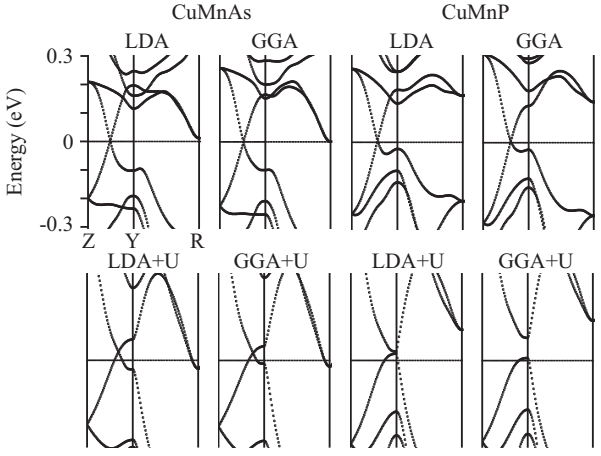

Fig. 9. Band structures of orthorhombic CuMnAs and CuMnP calculated using the depicted density-functional theories.

in which the gap opens in CuMnP. The spectra are consistent with common trends in III–V semiconductors of larger band gaps for lighter group-V elements and with the expected enhancement of the calculated semiconductor gap due to both the GGA correction to the local density theory and the correlation effects on Mn *d*-orbitals. Since the effects of these corrections are relatively strong, it might be desirable to employ in future studies computational methods which go beyond the GGA+U approximation in order to get a more quantitative understanding of the electronic structure of the high-temperature CuMn–V AFMs.

5. Conclusions

We have performed a combined experimental and theoretical study of magnetic and electronic properties of CuMn–V compounds which complements previous work on alkali-metal based I(a)–Mn–V AFM semiconductors and which is motivated by the search for suitable materials for semiconductor spintronic devices operating at room temperature. We observe experimentally a transition from a low Néel temperature AFM CuMnSb to a room-temperature AFM CuMnAs. Based on density-functional theory calculations, we ascribe the observation to the transition from the magnetically frustrated cubic half-Heusler structure of CuMnSb to the layered orthorhombic crystal structure of CuMnAs which lacks the magnetic frustration. Our calculations predict room-temperature antiferromagnetism also for CuMnP compound which has the same orthorhombic crystal structure as CuMnAs. The analysis of the calculated electronic structures of the CuMn–V compounds suggests that while CuMnSb is a semimetal, CuMnAs is at the transition from a semimetal to a semiconductor and CuMnP is a semiconductor with a positive band-gap across the entire Brillouin zone. Since CuMn–V compounds are stable and readily compatible with common epitaxial growth techniques of high-quality semiconductor structures, they represent favorable material systems for realizing high-temperature AFM-based spintronic devices with tunable electronic properties.

Acknowledgments

We thank C. Frontera and V. Holý for useful discussions, and M. Maryško and J. Prokleška for experimental assistance and we acknowledge support from EU Grant FP7-215368 SemiSpinNet, and ERC Advanced Grant 268066, from Czech Republic Grants P204/11/P339, P204/11/P339, AV0Z10100520, AV0Z10100521, IAA100100912, LC510, and Preamium Academiae.

References

[1] B.G. Park, J. Wunderlich, X. Marti, V. Holy, Y. Kurosaki, M. Yamada, H. Yamamoto, A. Nishide, J. Hayakawa, H. Takahashi, A.B. Shick, T. Jungwirth, A spin-valve-like magnetoresistance of an antiferromagnet-based tunnel junction, Nature Materials 10 (2011) 347.
[2] R.H. Forster, G.B. Johnston, D.A. Wheeler, Studies on the Heusler alloys-III. The antiferromagnetic phase in the Cu–Mn–Sb system, Journal of Physics and Chemistry of Solids 29 (1968) 855.
[3] K. Endo, Magnetic studies of Cl_b-compounds CuMnSb, PdMnSb and Cu_{1-x}(Ni or Pd)$_x$ MnSb, Journal of the Physical Society of Japan 29 (1970) 643.
[4] S.S. Abdulnoor, F.M.J. Ali, J. Leciejwicz, Magnetic phase transition of the $Cu_{1-x}Pd_x$MnSb system, Journal of Magnetism and Magnetic Materials 15–18 (1980) 475.
[5] T. Jeong, R. Weht, W.E. Pickett, Semimetallic antiferromagnetism in the half-Heusler compound CuMnSb, Physical Review B 71 (2005) 184103.
[6] J. Boeuf, C. Pfleiderer, A. Faisst, Low-temperature properties of the semi-Heusler compound CuMnSb, Physical Review B 74 (2006) 024428.
[7] N.P. Duong, L.T. Hunga, T.D. Hiena, N.P. Thuy, N.T. Trung, E. Brück, Magnetic properties of half-metallic semi Heusler $Co_{1-x}Cu_x$MnSb compounds, Journal of Magnetism and Magnetic Materials 311 (2007) 605.
[8] I. Galanakis, E. Sasioglu, K. Özdogan, Magnetic phase transition in half-metallic CoMnSb and NiMnSb semi-Heusler alloys upon Cu doping: first-principles calculations, Physical Review B 77 (2008) 214417.
[9] J. Mündelein, H.U. Schuster, Preparation and crystal structure of compounds MnCuX (X=P, As, P_xAs_{1-x}), Zeitschrift für Naturforschung B 47 (1992) 925.
[10] W. Bronger, P. Müller, R. Höppner, H.U. Schuster, The magnetic properties of NaMnP, NaMnAs, NaMnSb, NaMnBi, LiMnAs, and KMnAs, characterized by neutron diffraction experiments, Zeitschrift für Anorganische und Allgemeine Chemie 539 (1986) 175.
[11] J. Rodríguez-Carvajal, Recent advances in magnetic structure determination by neutron powder diffraction, Physica B 192 (1993) 55.

[12] P. Blaha, K. Schwarz, G.K.H. Madsen, D. Kvasnicka, J. Luitz, An Augmented Plane Save + Local Orbitals Program for Calculating Crystal Properties, ISBN 3-9501031-1-2 (Karlheinz Schwarz, Techn. Universität Wien, Austria, 2001).
[13] J.P. Perdew, K. Burke, M. Ernzerhof, Generalized gradient approximation made simple, Physical Review Letters 77 (1996) 3865.
[14] T. Jungwirth, V. Novák, X. Marti, M. Cukr, F. Máca, A.B. Shick, J. Mašek, P. Horodyská, P. Němec, V. Holý, J. Zemek, P. Kužel, I. Němec, B.L. Gallagher, R.P. Campion, C.T. Foxon, J. Wunderlich, Demonstration of molecular beam epitaxy and a semiconducting band structure for I–Mn–V compounds, Physical Review B 83 (2011) 035321.
[15] E.L. Nagaev, Ferromagnetic and antiferromagnetic semiconductors, Soviet Physics Uspekhi 18 (1975) 863.
[16] K. Suzuki, H. Morita, T. Kaneko, H. Yoshida, H. Fujimori, Crystal structure and magnetic properties of the compound FeN, Journal of Alloys Compounds 201 (1993) 11.
[17] X. Chen, A. Hochstrat, P. Borisov, W. Kleemann, Successive antiferromagnetic phase transitions in α-MnS probed by the exchange bias effect, Applied Physics Letters 94 (2009) 032506.
[18] B. Westerstrandh, L. Lundgren, U. Gafvert, B. Carlsson, Magnetic susceptibility resistivity and thermal expansion measurements on FeP, Physica Scripta 15 (1977) 276.
[19] K. Selte, A. Kjekshus, A. Andresen, Magnetic structure and properties of FeAs, Acta Chemica Scandinavica 26 (1972) 3101.
[20] P.J. Picone, P.E. Clark, Magnetic ordering of interstitial iron in $Fe_{1+x}Sb$ alloys, Journal of Magnetism and Magnetic Materials 25 (1981) 140.
[21] E. Kaldis, G. von Schulthess, P. Wachter, Electrical resistivity of antiferromagnetic GdP, Solid State Communications 17 (1975) 1401.
[22] D.X. Li, Y. Haga, H. Shida, T. Suzuki, T. Koide, G. Kido, Magnetic behavior of stoichiometric and nonstoichiometric GdAs single crystals, Physical Review B 53 (1996) 8473.
[23] F.P. Missell, R.P. Guertin, S. Foner, Magnetic properties of NdSb, GdSb, TbSb, DySb, HbSb and ErSb under hydrostatic pressure, Solid State Communications 23 (1977) 369.
[24] M. Mekata, N. Yaguchi, T. Takagi, T. Sugino, S. Mitsuda, H. Yoshizawa, N. Hosoito, T. Shinjo, Successive magnetic ordering in $CuFeO_2$—a new type of partially disordered phase in a triangular lattice antiferromagnet, Journal of Physical Society of Japan 62 (1993) 4474.
[25] S. Esmaeilzadeh, U. Halenius, M. Valldor, Crystal growth, magnetic, and optical properties of the ternary nitride $MnSiN_2$, Chemical Material 18 (2006) 2713.
[26] J. Lamazares, F. Gonzalez-Jimenez, E. Jaimes, L. D'Onofrio, R. Iraldi, G. Sanchez-Porras, M. Quintero, J. Gonzalez, J.C. Woolley, G. Lamarche, Magnetic, transport, X-ray diffraction and Mössbauer measurements on $CuFeSe_2$, Journal of Magnetism and Magnetic Materials 104–107 (1992) 997.
[27] A. Rivas, F. Gonzalez-Jimenez, L. D'Onofrio, E. Jaimes, M. Quintero, J. Gonzalez, Mössbauer measurements in $CuFeTe_2$, Hyperfine Interactions 113 (1998) 493.
[28] F. Schucht, A. Dascoulidou, R. Muller, W. Jung, H.U. Schuster, W. Bronger, P. Muller, The magnetic properties of the alkali metal manganese pnictides KMnP, RbMnP, CsMnP, RbMnAs, KMnSb, KMnBi, RbMnBi, and CsMnBi—neutron diffraction and susceptibility measurements, Zeitschrift für Anorganische und Allgemeine Chemie 625 (1999) 31.
[29] V.I. Anisimov, I.V. Solovyev, M.A. Korotin, M.T. Czyzyk, G.A. Sawatzky, Density-functional theory and NiO photoemission spectra, Physical Review B 48 (1993) 16929.
[30] A.I. Liechtenstein, V.I. Anisimov, J. Zaanen, Density-functional theory and strong interactions: orbital ordering in Mott–Hubbard insulators, Physical Review B 52 (1995) R5467.
[31] J.P. Perdew, Y. Wang, Accurate and simple analytic representation of the electron-gas correlation energy, Physical Review B 45 (1992) 13244.